We are IntechOpen, the world's leading publisher of Open Access books Built by scientists, for scientists

6,900
Open access books available

185,000
International authors and editors

200M
Downloads

Our authors are among the

154
Countries delivered to

TOP 1%
most cited scientists

12.2%
Contributors from top 500 universities

WEB OF SCIENCE™

Selection of our books indexed in the Book Citation Index in Web of Science™ Core Collection (BKCI)

Interested in publishing with us?
Contact book.department@intechopen.com

Numbers displayed above are based on latest data collected.
For more information visit www.intechopen.com

Chapter 10

Rock Magnetic Properties of Sedimentary Rocks in Central Hokkaido — Insights into Sedimentary and Tectonic Processes on an Active Margin

Yasuto Itoh, Machiko Tamaki and Osamu Takano

Additional information is available at the end of the chapter

http://dx.doi.org/10.5772/56650

1. Introduction

Reflecting a complicated subduction and collision history on the eastern Eurasian margin, central Hokkaido has been a site of various types of basin formation. Thick piles of the Cretaceous and Paleogene sediments (Figure 1; [1]) buried a regional forearc basin subducted by the Izanagi/Kula and Pacific Plates. Paleomagnetic studies of the Cretaceous Yezo Supergroup [2,3] showed that the present forearc is divided into some basins developed in different areas. Sedimentary system and forearc basin architecture in the Paleogene was studied in detail by Takano and Waseda [4] and Takano et al. [5].

Under the influence of arc-arc collision on the Pacific convergent margin, vigorous mountain building and formation of foreland basins became active since the late Cenozoic. The Ishikari-Teshio belt (see Figure 2) is underlain with thick middle Miocene clastic strata. These are the Kawabata and its correlative formations, derived from the longitudinal mountainous ranges that were uplifted and eroded during that time [6]. It is generally regarded as a typical foreland setting, and the burial history of turbidites and associated coarse clastics of the Kawabata Formation has previously been studied from a sedimentological viewpoint (e.g., [7]). The process through which the Miocene basin developed in central Hokkaido is not only governed by compressive stress in the collision zone, but also by coeval tectonic events like back-arc spreading in the Japan Sea (e.g., [8]) and dextral transcurrent faulting along the Eurasian margin (e.g., [9]).

In this paper, we present preliminary results of rock magnetic analyses of the Cretaceous Yezo Supergroup, the Eocene Ishikari Group and the Miocene Kawabata Formation in order to detect tectonic movements around the basin and to describe the microfabric of sedimentary

INTECH
open science | open minds

© 2013 Itoh et al.; licensee InTech. This is an open access article distributed under the terms of the Creative Commons Attribution License (http://creativecommons.org/licenses/by/3.0), which permits unrestricted use, distribution, and reproduction in any medium, provided the original work is properly cited.

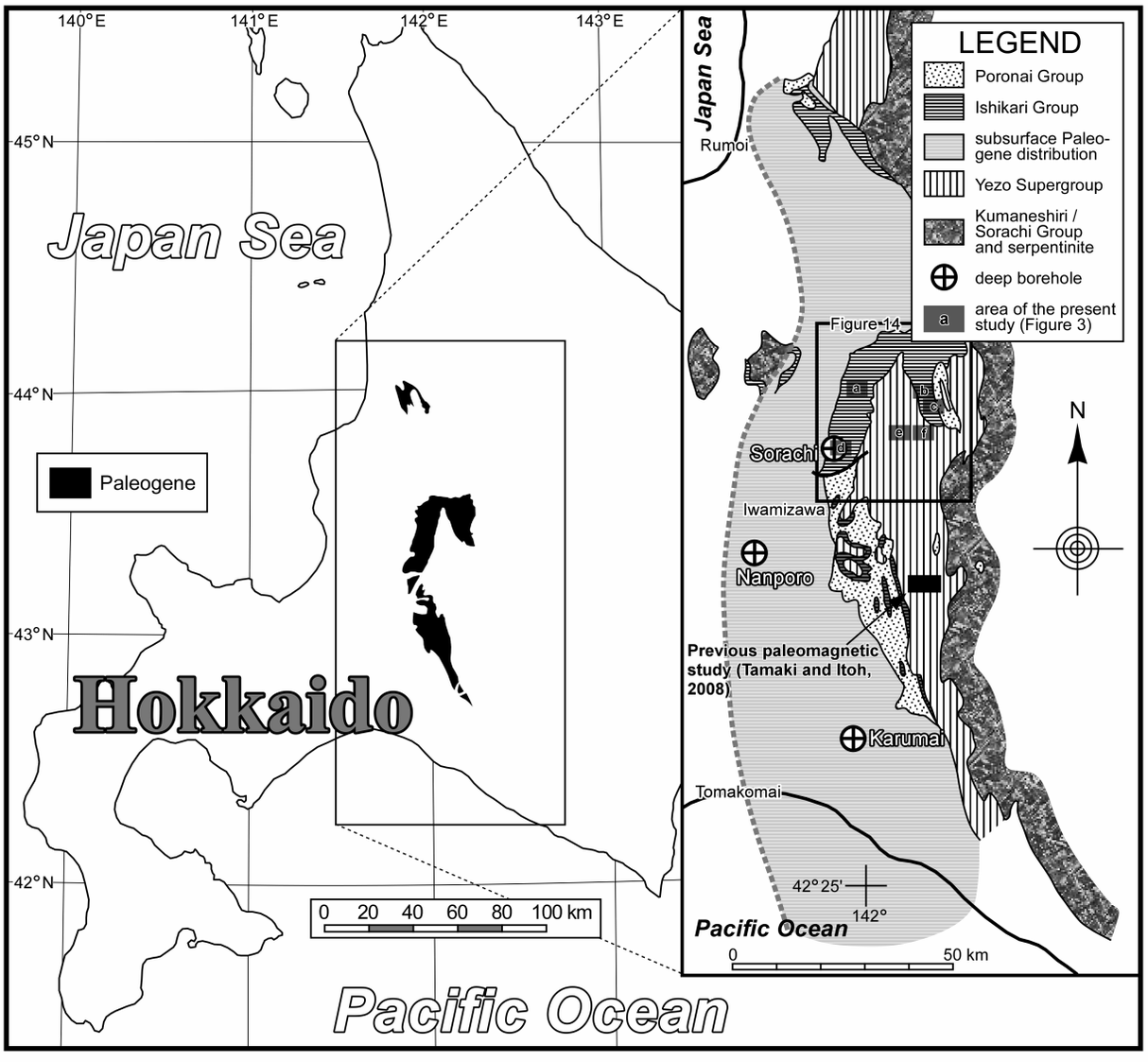

Figure 1. Index map of the study area of the Cretaceous and Paleogene strata. Geologic map is after Editorial Committee of Hokkaido, Regional Geology of Japan [1]

rocks related to the tectonic regime and sedimentation processes in the mobile zone. This study is an attempt to apply magnetic properties to tectono-sedimentology.

2. Geology

2.1. Background

The Yezo Supergroup deposited on the Cretaceous forearc and consists of monotonous mudstone intercalated by coarse clastics and ash layers. After a stagnant subsidence stage at the beginning of the Cenozoic, fluvial sediments of the Ishikari Group and its correlative units

http://dx.doi.org/10.5772/56650

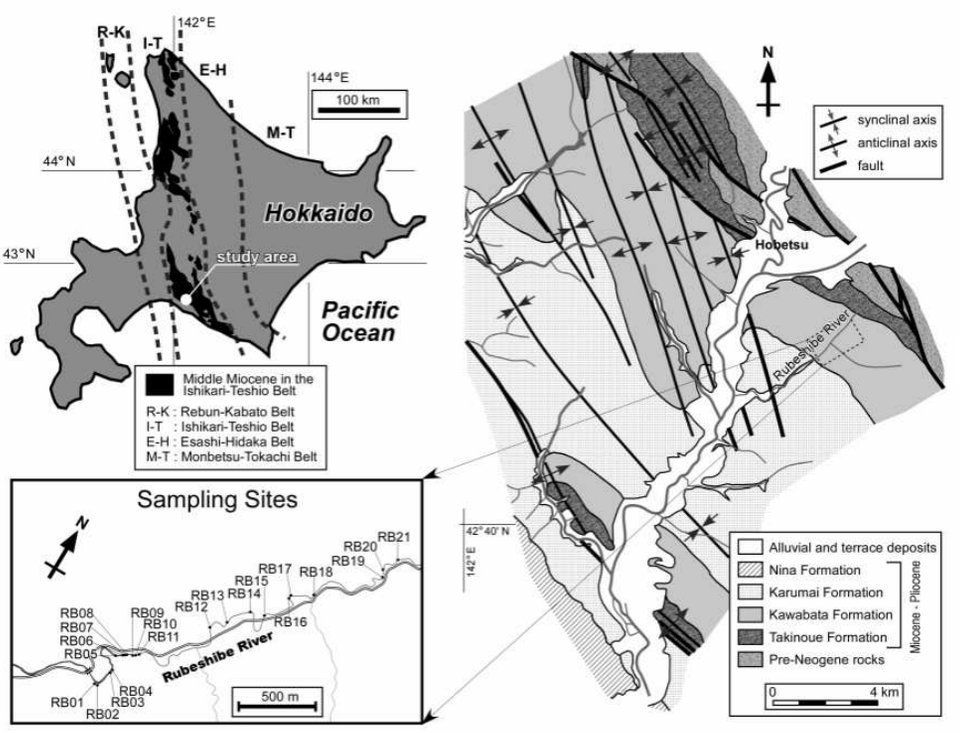

Figure 2. Cenozoic tectonic context of Hokkaido, geology of the study area of the Neogene strata (simplified from Kawakami et al. [7]), and locations of rock magnetic samples

began to bury depressions on the forearc. As a result of strong deformation and continued sedimentation on the active margin, surface distribution of the Eocene Ishikari Group is rather restricted. However, numerous exploration drilling clarified that voluminous Paleogene units are concealed under the alluvial plain (Figure 1). Paleogene depositional sequence and facies classification were described by Takano et al. [5]. They are shown in Figure 3 using abbreviations.

The study area of the Kawabata Formation is located in the southern part of the middle Miocene basins of the Ishikari-Teshio belt. Folded sedimentary units are distributed with a NNW-SSE trend, and are cut by numerous faults (Figure 2). The area is divided into the following formations in ascending order [7]: the Takinoue Formation, the Kawabata Formation, the Karumai Formation, and the Nina Formation (Figure 4). They represent the sequence by which an elongate N-S foreland basin was filled. The middle Miocene Kawabata Formation comprises mainly turbidites and associated coarse clastic rocks derived from the eastern hinterland [7].

2.2. Sedimentary facies of the Miocene unit

This study conducted sedimentary facies analysis for the Kawabata Formation along the Rubeshibe River (Figure 2). The analysis revealed that the turbidites of the Kawabata Formation mainly consisted of sheet-flow turbidite facies association and channel-levee facies association (Figure 5). The sheet-flow turbidite facies association comprises aggradational stacking of rhythmic alternating beds of turbidite sandstone and mudstone with rare upward

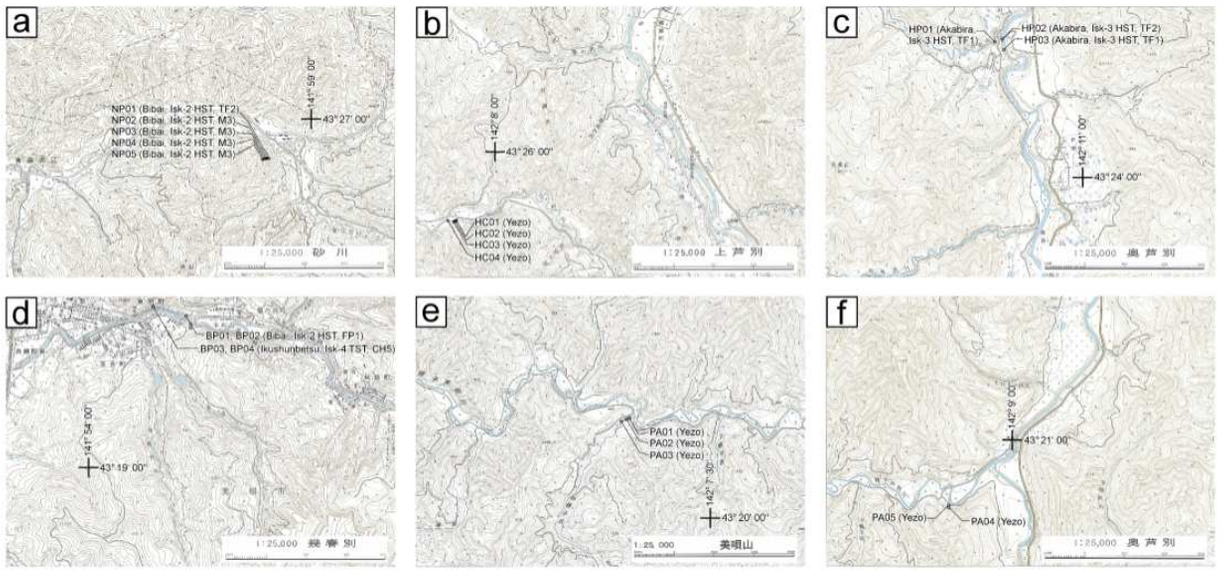

Figure 3. Sampling localities for rock magnetic analyses of the Cretaceous and Paleogene strata. The base maps are parts of the "Sunagawa", "Kamiashibetsu", "Okuashibetsu", "Ikushunbetsu" and "Bibaiyama" 1:25,000 topographic maps published by the Geographical Survey Institute. As for the Paleogene sites (a, c and d), geologic units (Yezo, Yezo Supergroup; Bibai, Bibai Formation; Akabira, Akabira Formation; Ikushunbetsu, Ikushunbetsu Formation), depositional sequence and facies classification are shown in parentheses after Takano et al. [5]

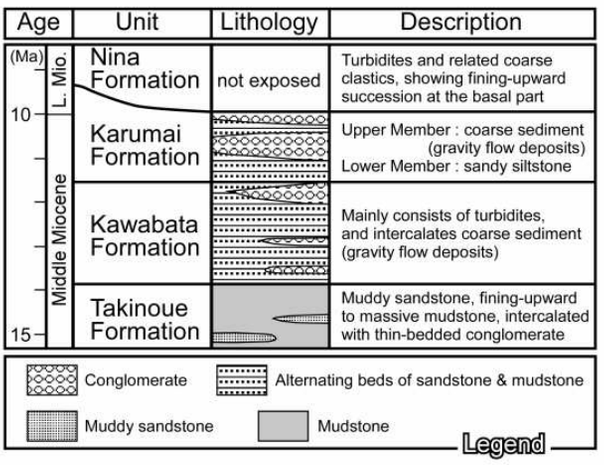

Figure 4. Neogene stratigraphy of the study area of the Kawabata Formation

thickening or thinning successions, and is interpreted to be sheet-like turbidites with minor occurrences of depositional lobes, which occupied major part of the trough-like foreland basin fill [7,10]. The channel-levee facies association is composed of thick amalgamated sandstone facies with slump blocks and thinly bedded alternating beds of sandstone and mudstone. These two facies appearing coupled is indicative of an elongated channel-levee system made of the main channel with levees on both sides. These two facies associations are believed to have been deposited in an elongated trough-like foredeep in the foreland basin [7]. The

http://dx.doi.org/10.5772/56650

turbidites of the Kawabata Formation commonly contain sedimentary structures indicating paleocurrent directions; e.g., sole marks (mostly flute marks) at the bottom of individual turbidite bed, and current ripples in Bouma Tc division [11].

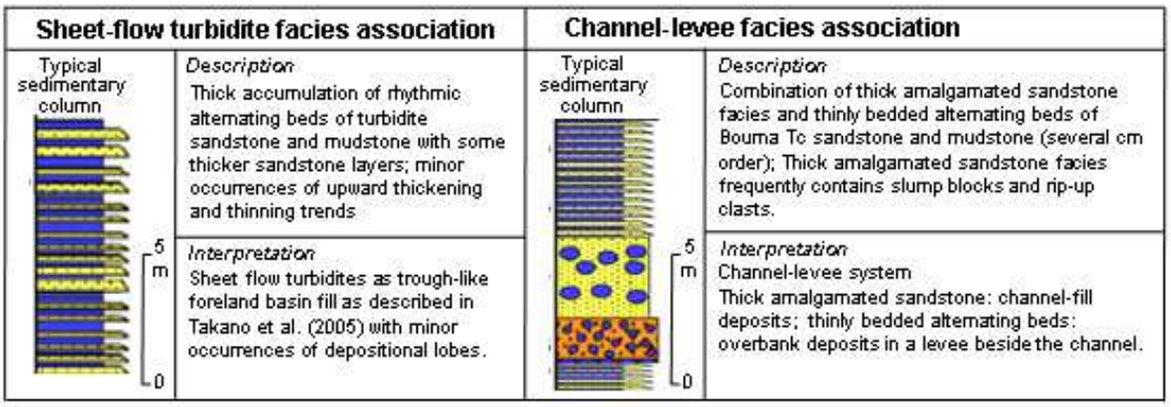

Figure 5. Facies association classification of the Kawabata Formation along the Rubeshibe River

3. Rock magnetism

We obtained samples for rock magnetic analyses exclusively from fine-grained parts of the target sedimentary units, since fine sedimentary rocks generally preserve stable detrital remanent magnetization (DRM). Few visible markers of the sedimentation process accompany such sediments, so we attempted to measure their microscopic magnetic fabric, which may be related to paleocurrent directions (e.g., [12]).

3.1. Basic measurements

The Cretaceous and Eocene samples were taken from outcrops along the streambed in central Hokkaido (Figure 3) using an engine or electric drill at 21 sites. Samples of the Kawabata Formation were collected with a battery-powered electric drill at 21 sites along the Rubeshibe River (Figure 2). The bedding attitudes were measured on outcrops to allow us to compensate for tectonic tilting later. Between seven and sixteen independently oriented cores 25 mm in diameter were obtained at each site using a magnetic compass. Cylindrical specimens 22 mm in length were cut from each core and the natural remanent magnetization (NRM) of each specimen was measured using a cryogenic magnetometer (model 760-R SRM, 2-G Enterprises). Low-field magnetic susceptibility was measured on a Bartington MS2 susceptibility meter, and the anisotropy of magnetic susceptibility (AMS) was measured using an AGICO KappaBridge KLY-3 S magnetic susceptibility meter. After the basic measurements, pilot specimens with average NRM intensities, directions and susceptibility levels were selected from each site for subsequent demagnetization tests.

3.2. Demagnetization tests

In order to isolate stable components of the remanent magnetization, progressive alternating field demagnetization (PAFD) and progressive thermal demagnetization (PThD) tests were carried out on two pilot specimens per site that had average NRM directions. The PAFD test loading ranged from 0 to 80 mT using a three-axis tumbling system with specimens contained in a μ-metal envelope. The PThD test was performed using an electric furnace, with a residual magnetic field less than 10 nT, beginning at 100 ºC and continuing until the specimen was either fully demagnetized and a characteristic remanent magnetization (ChRM) component was isolated, or until the thermal treatment provoked erratic behavior of the magnetic direction. Specimens' low-field bulk magnetic susceptibilities were measured using a susceptibility meter after each PThD step in order to monitor chemical changes in ferromagnetic minerals.

Figure 6 presents typical PThD and PAFD results for the Yezo Supergroup and Ishikari Group. It is obvious that the ChRM direction was not isolated because of unstable behavior in thermal treatment (Figure 6a), overlapping spectra of primary and secondary magnetization (Figure 6b) and partial remagnetization within a site (Figure 6c,d). Therefore further analyses for magnetic granulometry were not applied on the Cretaceous and Eocene samples. On the other hand, PThD treatment was effective for isolating stable ChRM in the sedimentary rocks of the Kawabata Formation. Figure 7 shows typical results of the progressive demagnetization tests.

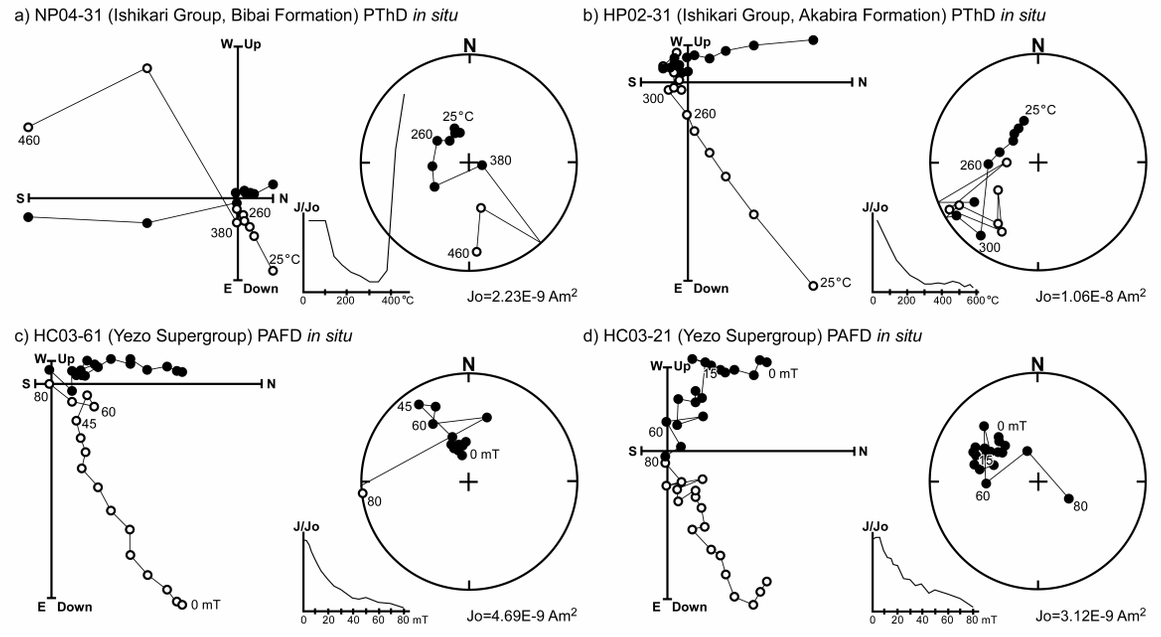

Figure 6. Typical results of progressive thermal demagnetization (PThD) and progressive alternating field demagnetization (PAFD) in geographic coordinates for the Paleogene Ishikari Group (a,b) and the Cretaceous Yezo Supergroup (c,d). On the vector-demagnetization diagrams, solid (open) circles are projection of vector end-points on horizontal (N-S vertical) plane. Equal-area projection and normalized intensity decay curve are shown on the right-side of each vector diagram. Solid (open) circles in equal-area nets are projections on the lower (upper) hemisphere. Numbers attached on data points are demagnetization levels in °C or mT

http://dx.doi.org/10.5772/56650

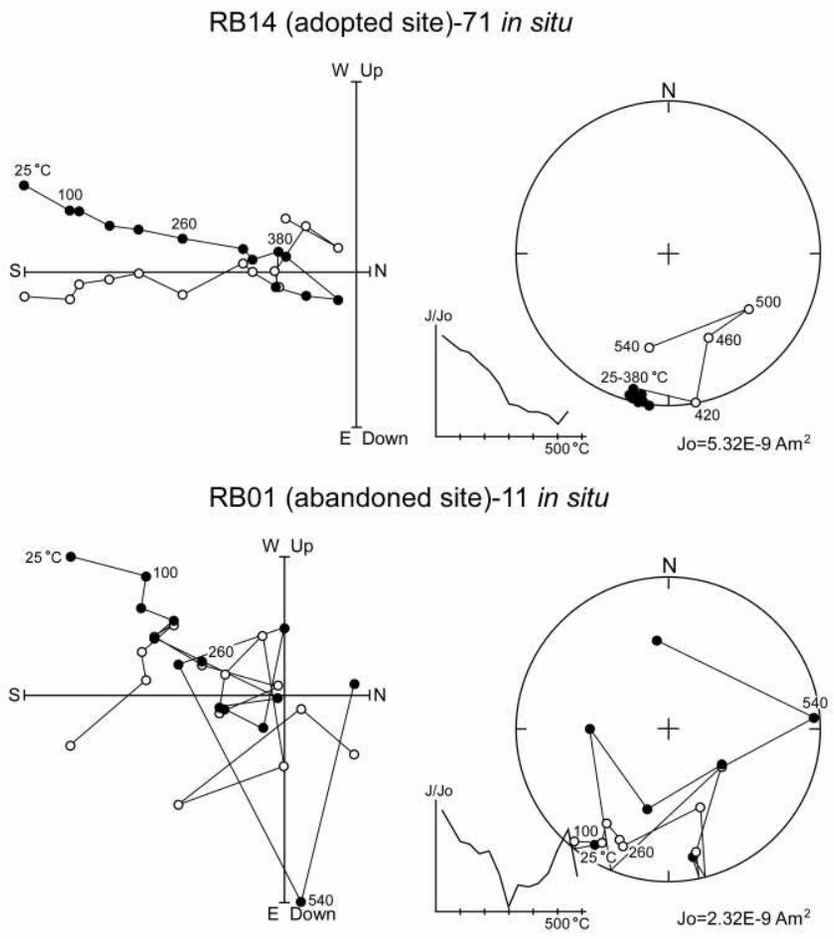

Figure 7. Results of progressive thermal demagnetization for samples of the Neogene Kawabata Formation with stable (upper) and unstable (lower) magnetization. All coordinates are geographic (*in situ*). Units are bulk remanent intensity. The solid and open circles in the vector-demagnetization diagrams (left) are projections of vector end-points on the horizontal and north-south vertical planes, respectively. The solid and open circles in the equal-area Schmidt nets (right) are projections on the lower and upper hemispheres, respectively

3.3. Hysteresis properties

Hysteresis parameters were determined for the Kawabata samples with an alternating gradient magnetometer (Princeton Measurements Corporation, MicroMag 2900). Ten sample chips up to 1 mm in size were randomly selected from site RB16, where stable ChRM has been successfully isolated. Figure 8 displays typical hysteresis of the Kawabata mudstones. The raw diagram seems to suggest the absence of ferromagnetic material. After correcting the linear gradient of paramagnetism, a weak ferromagnetic behavior signature can be recognized. Saturation magnetization (Js), saturation remanence (Jrs) and coercive force (Hc) values were determined for all samples from their hysteresis loops. Their relatively low Hc (~ 100 mT) implies that magnetite is the dominant remanence carrier. After acquiring coercivity of remanence (Hcr) values through backfield demagnetization experiments, we constructed a correlation plot of Jrs/Js versus Hcr/Hc [13] as shown in Figure 9. All the data are plotted in the pseudo-single domain (PSD) region of magnetite.

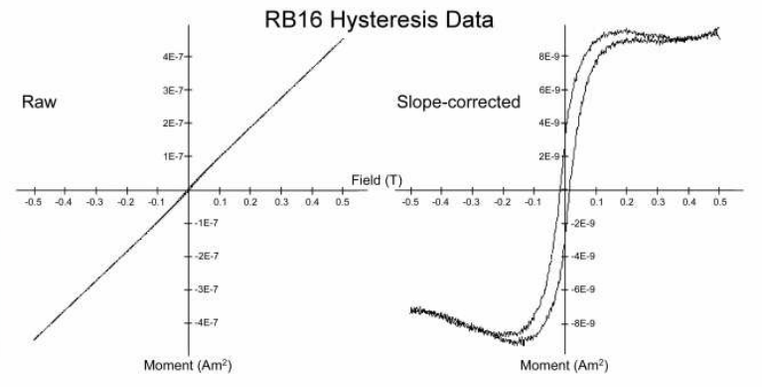

Figure 8. An example of hysteresis loop for a sample of the Kawabata Formation from site RB16 (Left: raw data, Right: data corrected for slope of paramagnetism)

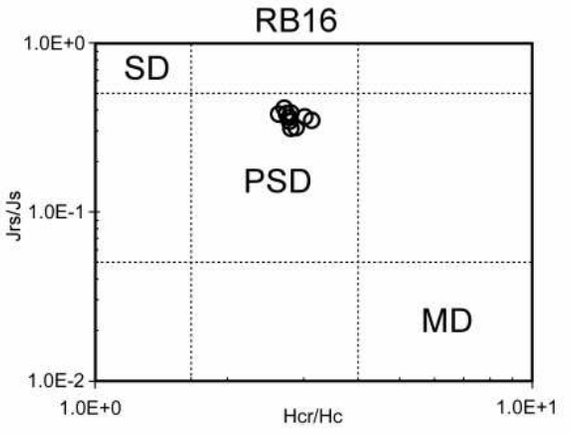

Figure 9. Logarithmic plot of hysteresis parameters [13] of ten samples of the Kawabata Formation from site RB16. Abbreviations: SD, single domain; PSD, pseudo-single domain; MD, multi-domain

4. Discussion

4.1. Rotational motions

We found stable magnetic components at three sites of the Kawabata Formation. Their directions were determined with a three-dimensional least squares analysis technique [14]. Figure 10 and Table 1 present site-mean ChRM directions obtained from the Kawabata Formation. They exhibit antipodal directions, and precision parameter (κ) improves after tilt correction. Although the number of data points is minimal for tectonic discussion, we can interpret the site-mean directions as a record of the Earth's dipole magnetic field, acquired before the strata tilted. The declination of the formation mean exhibits a significant westerly deflection, which suggests counterclockwise rotation of the study area.

http://dx.doi.org/10.5772/56650

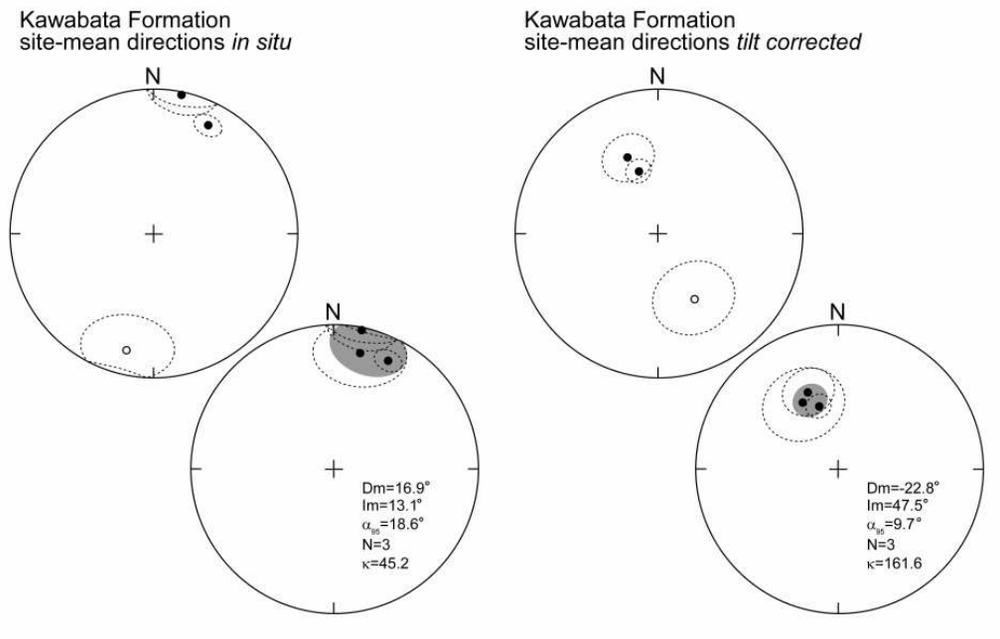

Figure 10. Site-mean ChRM directions of the Kawabata Formation in the study area. The solid and open circles in all the equal-area nets are projections on the lower and upper hemispheres, respectively. Dotted ovals show 95 % confidence limits. Lower diagrams are polarity-converted for calculating formation mean directions and Fisher's precision parameters as annotated in the diagrams (Shaded ovals depict 95 % confidence for the formation means)

Site	Latitude	Longitude	D	I	Dc	Ic	α_{95}	κ	N	ϕ	λ
RB14	42.7361	142.1771	-167.1	-18.7	151.2	-47.0	21.9	13.1	5	62.5	29.5
RB16	42.7379	142.1793	11.4	2.8	-21.8	42.5	14.0	14.4	9	64.5	13.9
RB17	42.7381	142.1793	26.8	17.4	-17.4	52.7	6.8	66.5	8	73.3	23.1

D and I, *in situ* site-mean declination and inclination before tilt correction in degrees, respectively; Dc and Ic, site-mean declination and inclination after tilt correction in degrees, respectively; α95, radius of 95% confidence circle in degrees; κ, precision parameter; N, number of specimens; ϕ and λ, latitude (N) and longitude (E) of north-seeking virtual geomagnetic pole for untilted site-mean direction in degrees, respectively.

Table 1. Paleomagnetic directions of the Kawabata Formation

A previous study [15] suggested a clockwise tectonic rotation around central Hokkaido based on a paleomagnetic study of the Kawabata Formation. Takeuchi et al. [16] proposed a coherent rotational model with 'domino-style' rigid crustal blocks. However, Tamaki et al. [17] criticized the block rotation scheme as being overly simplistic based on differential rotations inferred from Oligocene paleomagnetic data. They restored crustal deformation in central Hokkaido using dislocation modeling, and found complicated vertical-axis rotations around terminations of the faults that contributed to the formation of N-S elongate sedimentary basins. Figure 11 demonstrates differential rotation in central Hokkaido since the middle Miocene.

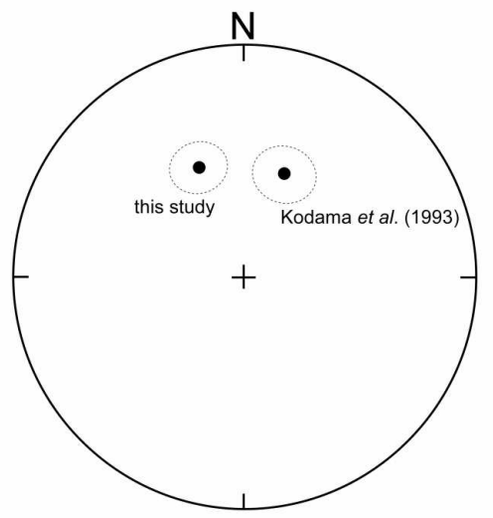

Figure 11. Comparison of the mean paleomagnetic directions of the Kawabata Formation in central Hokkaido between this study and [15]. Data are plotted on the lower hemisphere of the equal-area projection. Dotted ovals represent 95 % confidence limits

4.2. Sedimentation process inferred from AMS fabric

We found that the AMS fabric (orientation of principal axes) were precisely determined at all the sampled localities. Tables 2 and 3 show the AMS parameters for the Cretaceous/Eocene units and the Miocene unit, respectively. Figure 12 delineates typical AMS fabric obtained from the Ishikari (left) and Yezo (right) samples. After tilt-correction, the maximum (K_1) and intermediate (K_2) axes of AMS are bound to the horizontal plane with a subtle imbrication suggestive of hydrodynamic forcing.

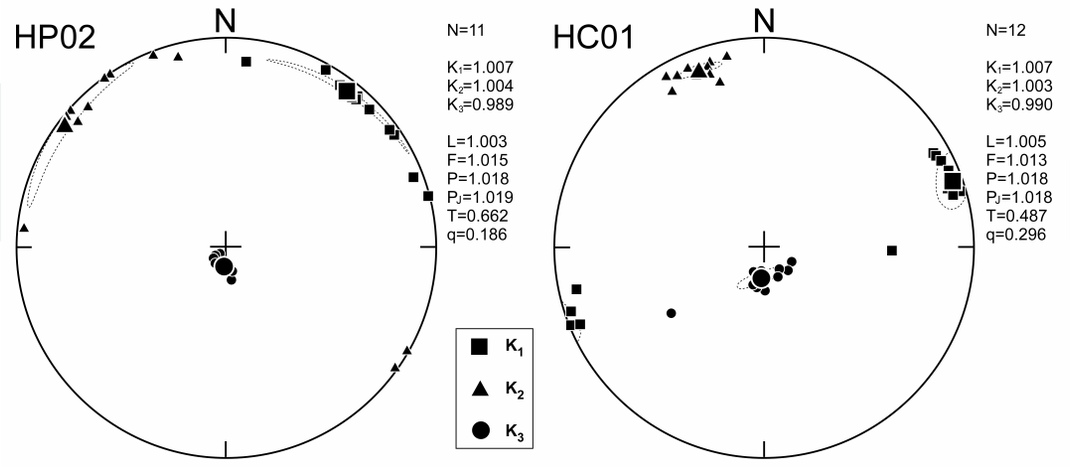

Figure 12. Anisotropy of magnetic susceptibility (AMS) fabric (principal susceptibility axes) for all specimens of typical sites of the Ishikari Group (HP02) and Yezo Supergroup (HC01) plotted on the lower hemisphere of equal-area projections. Data are shown in stratigraphic coordinates. Ovals surrounding mean directions of three axes (shown by larger symbols) are 95% confidence regions. See Table 2 for all the AMS parameters

http://dx.doi.org/10.5772/56650

Site	*N*	K_1 Str. (D, I)	K_2 Str. (D, I)	K_3 Str. (D, I)	*L* (K_1/K_2)	*F* (K_2/K_3)	*P* (K_1/K_3)	P_J	*T*	*q*	Unit / Sequence
Paleogene											
BP01	11	1.010	1.005	0.984	1.005	1.021	1.026	1.028	0.619	0.213	Bb / Isk-2HST
		(207, 4)	(297, 1)	(35, 86)							
BP02	11	1.009	1.008	0.982	1.001	1.026	1.027	1.031	0.917	0.043	Bb / Isk-2HST
		(226, 3)	(136, 4)	(0, 85)							
BP03	11	1.010	1.005	0.985	1.005	1.020	1.025	1.027	0.593	0.229	Ik / Isk-4TST
		(233, 9)	(141, 7)	(16, 78)							
BP04	13	1.010	1.002	0.988	1.008	1.014	1.022	1.022	0.259	0.458	Ik / Isk-4TST
		(225, 6)	(134, 3)	(15, 83)							
HP01	18	1.010	1.004	0.987	1.006	1.017	1.023	1.024	0.479	0.303	Ak / Isk-3HST
		(271, 4)	(180, 8)	(29, 81)							
HP02	11	1.007	1.004	0.989	1.003	1.015	1.018	1.019	0.662	0.186	Ak / Isk-3HST
		(38, 6)	(307, 4)	(187, 83)							
NP01	15	1.009	1.006	0.985	1.003	1.022	1.025	1.027	0.762	0.128	Bb / Isk-2HST
		(264, 2)	(174, 7)	(11, 83)							
NP02	9	1.013	1.006	0.981	1.006	1.026	1.032	1.034	0.597	0.227	Bb / Isk-2HST
		(252, 10)	(162, 2)	(59, 80)							
NP03	10	1.006	1.004	0.989	1.002	1.016	1.018	1.019	0.779	0.118	Bb / Isk-2HST
		(253, 1)	(163, 7)	(349, 83)							
NP04	7	1.009	1.006	0.985	1.002	1.022	1.024	1.027	0.791	0.111	Bb / Isk-2HST
		(80, 10)	(170, 4)	(282, 79)							
NP05	9	1.007	1.003	0.990	1.004	1.013	1.017	1.018	0.536	0.264	Bb / Isk-2HST
		(39, 28)	(141, 21)	(261, 54)							
Cretaceous											
HC01	12	1.007	1.003	0.990	1.005	1.013	1.018	1.018	0.487	0.296	
		(71, 5)	(340, 11)	(187, 78)							
HC02	10	1.011	1.005	0.984	1.006	1.021	1.027	1.028	0.541	0.262	
		(66, 2)	(156, 4)	(315, 86)							
HC03	11	1.010	1.002	0.988	1.008	1.014	1.022	1.022	0.274	0.447	
		(51, 4)	(321, 11)	(163, 78)							
PA01	13	1.006	1.003	0.991	1.003	1.012	1.015	1.016	0.650	0.193	
		(336, 11)	(70, 19)	(217, 68)							
PA04	14	1.017	1.014	0.969	1.004	1.046	1.049	1.055	0.852	0.078	
		(8, 9)	(99, 11)	(240, 76)							

N denotes the number of specimens. Directions of AMS principal axes are in stratigraphic coordinates. Abbreviations for the Paleogene geologic units: Ak, Akabira Formation; Bb, Bibai Formation; Ik, Ikushunbetsu Formation. Depositional sequence is after Takano & Waseda [4] and Takano et al. [5].

Table 2. Site-mean AMS parameters of the Paleogene and Cretaceous units in central Hokkaido

Figure 13 delineates typical AMS fabrics of the Kawabata Formation. Site RB08 typifies an elongate (prolate) fabric reflecting aligned detrital grains. Site RB14 has highly oblate fabric, as shown by a positive *T* parameter near unity. This fabric is essentially confined to the bedding plane under gravitational force. As the hysteresis study showed a negligible amount of ferromagnetic material in the Kawabata samples (Figure 8), we consider the AMS fabric as being governed simply by the shape anisotropy of paramagnetic minerals, i.e. alignments of elongate or platy grains such as amphibole or mica.

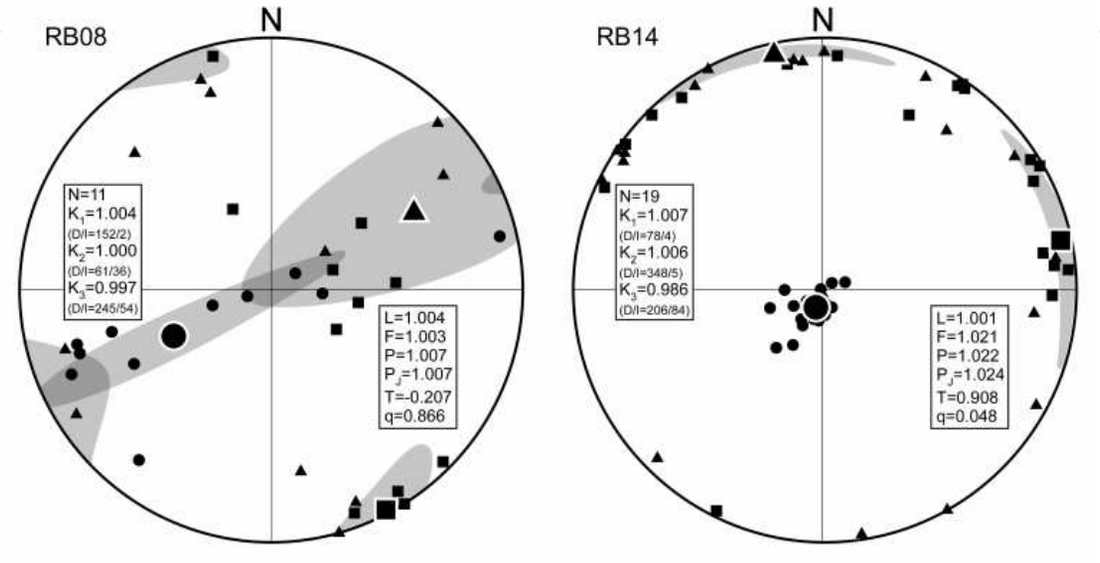

Figure 13. Typical tilt-corrected AMS fabric for the Kawabata Formation muddy samples. Prolate (left) and oblate (right) fabrics are numerically described by negative and positive T parameters, respectively, posted on the equal-area diagrams. All the data are plotted on the lower hemisphere. Square, triangular and circular symbols represent orthogonal maximum (K_1), intermediate (K_2), and minimum (K_3) AMS principal axes, respectively, and larger symbols show their mean directions. Shaded areas are 95 % confidence limits based upon Bingham statistics

Site	N	K_1 (D, I)	K_2 (D, I)	K_3 (D, I)	L (K_1/K_2)	F (K_2/K_3)	P (K_1/K_3)	P_J	T	q
RB01	11	1.013	1.006	0.981	1.007	1.025	1.033	1.034	0.546	0.260
		(16, 6)	(107, 7)	(242, 81)						
RB02	11	1.007	1.003	0.991	1.004	1.012	1.016	1.017	0.508	0.282
		(3, 20)	(98, 11)	(215, 66)						
RB03	12	1.006	1.002	0.992	1.004	1.010	1.014	1.015	0.475	0.304
		(326, 11)	(58, 11)	(190, 74)						
RB04	13	1.008	1.002	0.990	1.005	1.013	1.018	1.019	0.406	0.352
		(159, 2)	(249, 6)	(52, 83)						
RB05	15	1.005	1.001	0.993	1.004	1.008	1.012	1.012	0.330	0.404
		(4, 19)	(101, 19)	(232, 62)						

http://dx.doi.org/10.5772/56650

Site	N	K_1 (D, I)	K_2 (D, I)	K_3 (D, I)	L (K_1/K_2)	F (K_2/K_3)	P (K_1/K_3)	P_J	T	q
RB06	14	1.007	1.001	0.992	1.005	1.009	1.014	1.015	0.256	0.459
		(336, 5)	(66, 7)	(208, 82)						
RB07	12	1.005	0.999	0.996	1.007	1.002	1.009	1.009	-0.459	1.151
		(135, 24)	(41, 9)	(291, 64)						
RB08	11	1.004	1.000	0.997	1.004	1.003	1.007	1.007	-0.207	0.866
		(152, 2)	(61, 36)	(245, 54)						
RB09	17	1.005	1.001	0.994	1.004	1.007	1.011	1.011	0.313	0.416
		(121, 1)	(31, 7)	(218, 83)						
RB10	10	1.010	1.007	0.983	1.003	1.024	1.027	1.030	0.777	0.120
		(343, 2)	(252, 12)	(84, 78)						
RB11	12	1.002	0.999	0.998	1.003	1.001	1.004	1.004	-0.410	1.090
		(313, 42)	(105, 45)	(210, 15)						
RB12	12	1.005	1.004	0.991	1.002	1.013	1.015	1.016	0.763	0.127
		(3, 6)	(93, 1)	(192, 84)						
RB13	9	1.004	1.002	0.994	1.001	1.009	1.010	1.011	0.732	0.144
		(119, 26)	(214, 11)	(325, 61)						
RB14	19	1.007	1.006	0.986	1.001	1.021	1.022	1.024	0.908	0.048
		(78, 4)	(348, 5)	(206, 84)						
RB15	12	1.009	1.004	0.986	1.005	1.018	1.023	1.024	0.558	0.251
		(188, 10)	(96, 10)	(324, 76)						
RB16	15	1.013	1.010	0.977	1.003	1.034	1.036	1.041	0.848	0.080
		(281, 4)	(11, 5)	(152, 83)						
RB17	14	1.009	1.003	0.987	1.006	1.016	1.022	1.023	0.455	0.318
		(292, 6)	(201, 6)	(66, 81)						
RB18	7	1.009	1.001	0.990	1.008	1.011	1.018	1.018	0.169	0.528
		(120, 1)	(30, 2)	(234, 87)						
RB19	13	1.012	1.003	0.985	1.009	1.018	1.028	1.028	0.324	0.411
		(26, 15)	(277, 50)	(127, 36)						
RB20	11	1.013	1.005	0.982	1.008	1.023	1.031	1.032	0.458	0.317
		(300, 19)	(205, 15)	(78, 66)						
RB21	17	1.015	1.005	0.980	1.010	1.026	1.036	1.037	0.433	0.335
		(215, 75)	(90, 9)	(358, 12)						

N is the number of specimens. Directions of AMS principal axes are in stratigraphic coordinates.

Table 3. Site-mean AMS parameters of the Kawabata Formation

Sedimentological context of the AMS fabric is demonstrated in Figures 14 and 15. Paleocurrent directions inferred from the Eocene AMS data tend to align in N-S azimuth (Figure 14), and accord with development process of the forearc basin [4]. Takano and Waseda [4] demonstrated that the Eocene paleo-Ishikari basin experienced differential subsidence during deposition. Such deformation may be related to longstanding strike-slip faulting around central Hokkaido [17], and tectono- / sedimentological context of the AMS fabric will be better evaluated in the light of quantitative study of basin-forming processes described in this book. For reliable interpretation of AMS data, it is necessary to assess properties of ferromagnetic minerals, such as composition, grain size and contribution to bulk magnetic susceptibility, as shown in this paper.

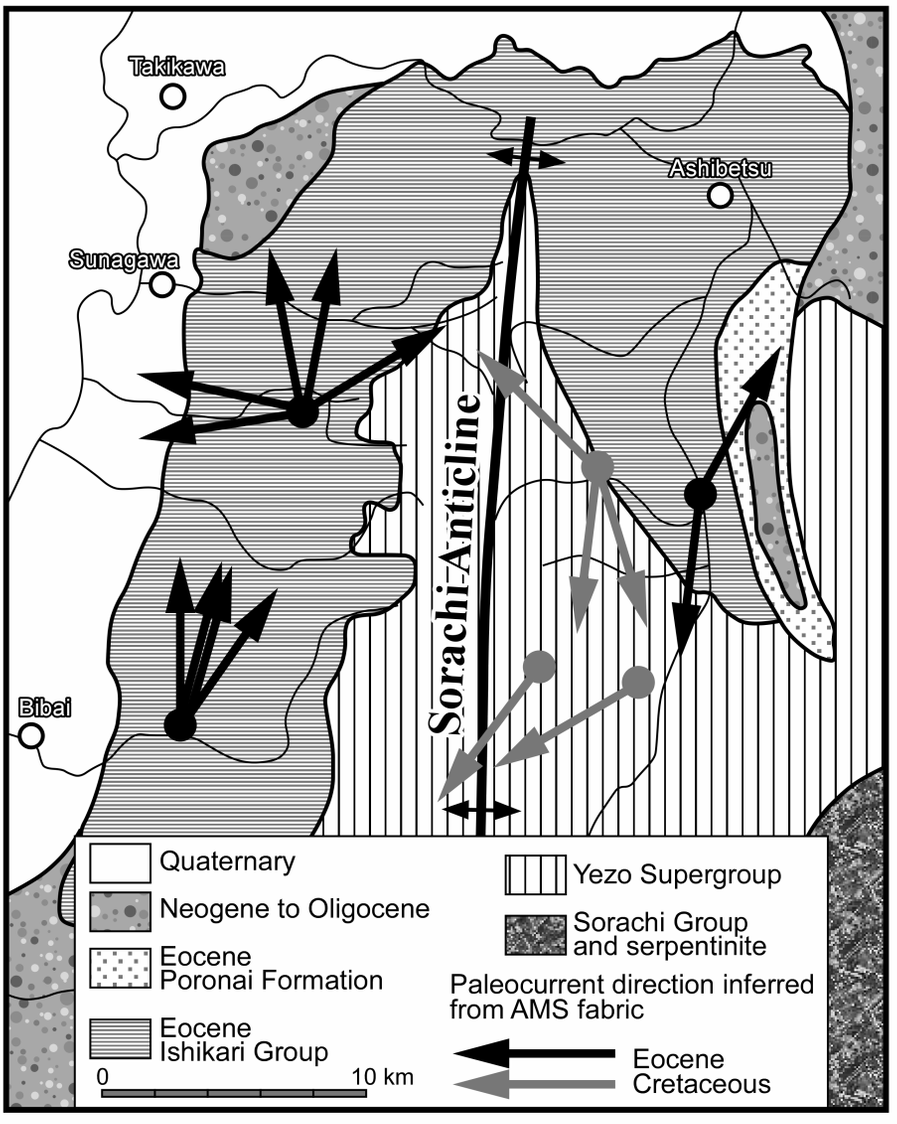

Figure 14. Paleocurrent directions inferred from AMS fabric of the Paleogene and Cretaceous samples. Geologic map is compiled from Editorial Committee of Hokkaido, Regional Geology of Japan [1] and Takano and Waseda [4]

http://dx.doi.org/10.5772/56650

Our field survey revealed indicators of paleocurrent directions in the Kawabata Formation along the Rubeshibe River as depicted in Figure 15. After correction for the counterclockwise rotation identified in our paleomagnetic study, most of the markers indicate a westward current direction with minor southward flow contributions. This is consistent with a tectono-sedimentary model of rapid burial of the Miocene N-S foreland basin by clastics derived from the eastern collision front presented in such research as Kawakami et al. [7]. Notably, the imbrication of the oblate AMS fabric matches visible sedimentary structures. Although the transport direction of muddy detrital material spilled out of a levee is not necessarily parallel to the turbidity current within a channel, AMS data can serve to indicate paleocurrents after the contributors to the magnetic fabric have been identified. Also note that K_1 of prolate samples (with negative T parameters) tend to align perpendicular to the paleocurrent direction, implying that elongate grains roll on the sediment surface.

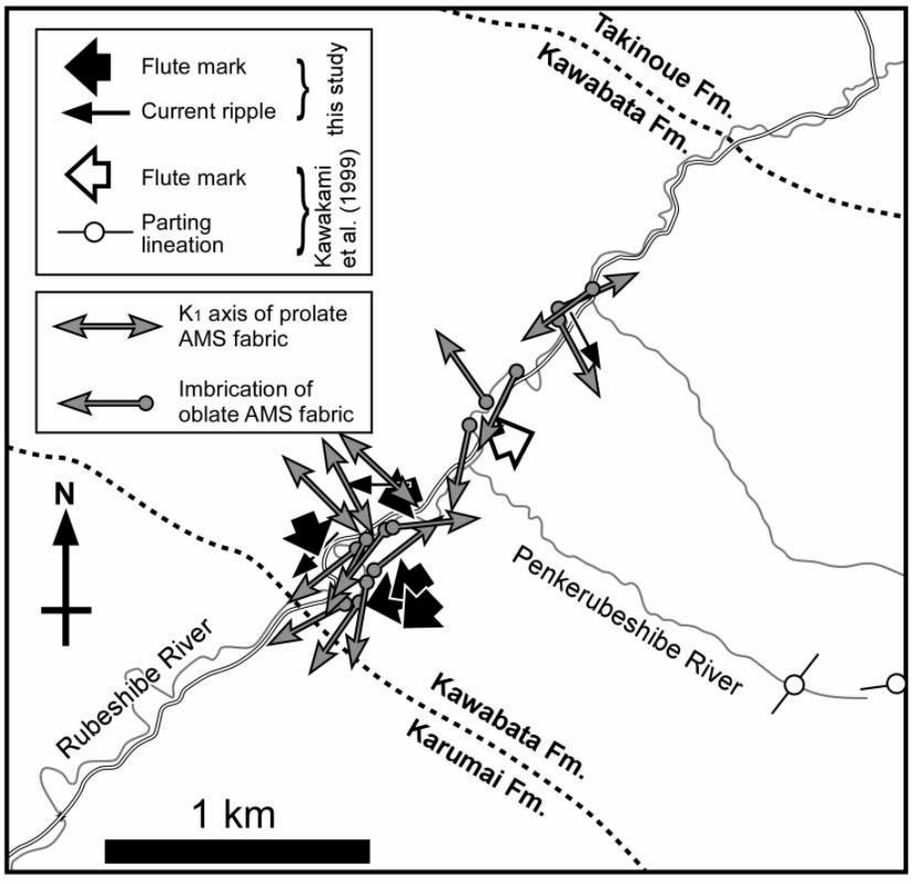

Figure 15. Paleocurrent map of the Kawabata Formation around the Rubeshibe River route. Formation boundaries are after Kawakami et al. [7]

Figure 16 delineates groups of microscopic fabrics identified in the Kawabata Formation as a function of the AMS shape parameter (T). The intensity of alignment forcing inferred from AMS data is closely related to sedimentary facies (shown on the right in the figure) determined by field observation. For example, weak hydrodynamic forcing corresponds to fine rhythmi-

cally alternating facies in channel-levee systems. Thus, the sedimentological context of muddy sediments' AMS fabric can be interpreted in the light of sandy sediments' facies analysis.

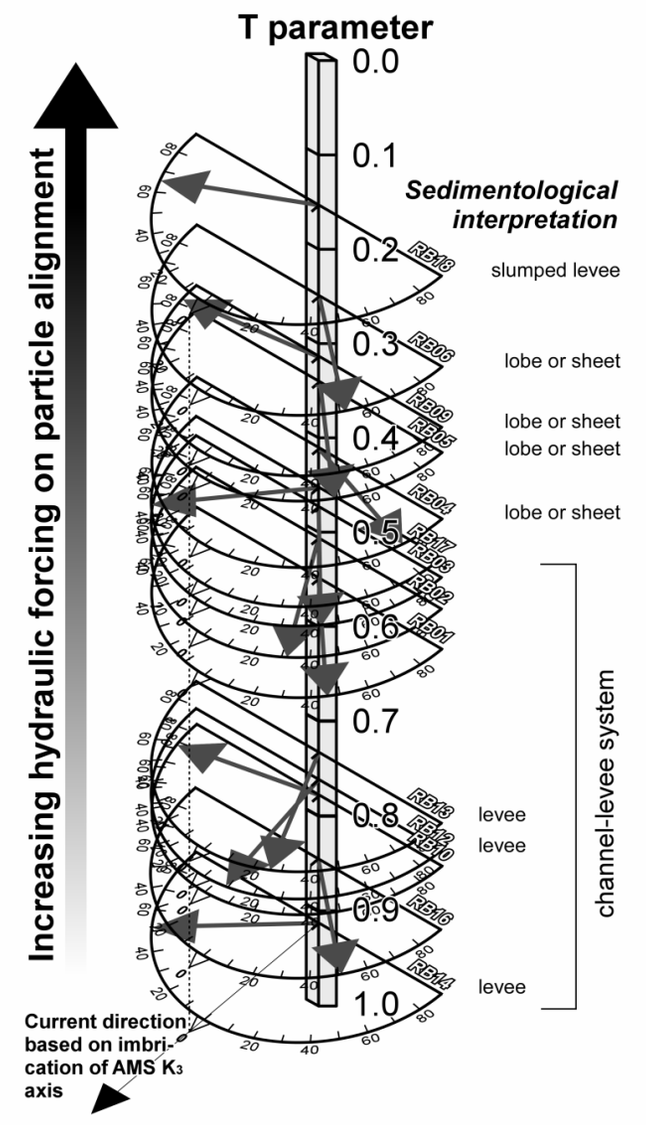

Figure 16. AMS paleocurrent indicators of the Kawabata Formation. Directions of K_1 (gray arrows) are shown as acute angles from the dotted baseline of K_3 axis imbrication. Vertical positions of the data are based on the T parameter. Samples with negative T values are excluded from the diagram because such cases have a large scatter in the K_3 directions

Azimuths of AMS maxima in natural sediments vary significantly, reflecting the size or shape of magnetic grains and changes in current velocities (e.g., [18]). Figure 16 presents the relationship between paleocurrent proxies estimated from the imbrication of the AMS minimum axis (K_3) and the K_1 trend. Tarling and Hrouda [19] stated that the angle between K_3 and K_1 changes as a function of current velocity and the slope of the sedimentary surface. Our result suggests that the orientation between those AMS sedimentary indicators can vary, regardless of the level of hydraulic forcing, based on the shape parameter (T), which implies development

http://dx.doi.org/10.5772/56650

of a preferred orientation. Although the AMS fabric is a diagnostic tool for patterns of sediment transportation, laboratory-based experiments that analyze natural sediments under conditions where a few of the prevailing factors are controlled, are essential to allow firm sedimentological interpretation of formation processes.

4.3. Re-deposition experiment and the origin of AMS

In order to consider the origin of the AMS in the Kawabata samples, we organized a re-deposition experiment. A silty sandstone (SP1C-1) and a mudstone (SP2F-1) samples were crushed and sieved into coarse, medium and fine fractions. The fine fraction (< 63 μm) was then separated into magnetic and non-magnetic fractions with an isodynamic separator. The 'magnetic' fraction actually contained no ferromagnetic opaque minerals such as magnetite, but had abundant biotite and common hornblende. It also contained garnet, probably derived from metamorphic rocks exposed around the hinterlands during the rapid deposition of the Miocene turbidite.

A suspension of the fine fraction was poured into a vertically settled plastic tube 1 m in length and 2.5 cm in diameter, filled with water. This deposit of artificial sediment was dehydrated at room temperature. After being soaked in an adhesive resin, the samples were trimmed into standard-sized specimens for rock-magnetic measurements. The AMS was measured with an AGICO KappaBridge KLY-3 S magnetic susceptibility meter. The AMS parameters for the artificial samples are summarized in Table 4.

Figure 17 presents the magnitudes of magnetic fabrics in natural sedimentary rocks and the re-deposited sediments of the Kawabata Formation. Obviously, the magnetic separation results in remarkable decrease of both the bulk susceptibility and the degree of anisotropy (P_J). It is also noteworthy that the shape parameter (T) of the artificial sediments is almost null, suggesting a neutral magnetic fabric. The directions of the principal AMS axes (see Table 4) are not bound to the horizontal plane or to geomagnetic north. Thus, the detrital particles, free from paramagnetic minerals having shape anisotropy, like platy biotite, are deposited without any gravitational or geomagnetic forcing, creating an isotropic sediment.

Sample	N	K_1 (D, I)	K_2 (D, I)	K_3 (D, I)	L (K_1/K_2)	F (K_2/K_3)	P (K_1/K_3)	P_J	T	q
SP1C-1	1	1.0009	1.0000	0.9992	1.001	1.001	1.002	1.002	-0.080	0.740
		(167, 75)	(265, 2)	(356, 15)						
SP2F-1	1	1.0014	1.0002	0.9984	1.001	1.002	1.003	1.003	0.180	0.517
		(250, 27)	(343, 6)	(84, 62)						

N is the number of specimens. Directions of principal axes of AMS are shown in *in situ* coordinates.

Table 4. AMS parameters of re-deposited non-magnetic fine fraction of the Kawabata Formation

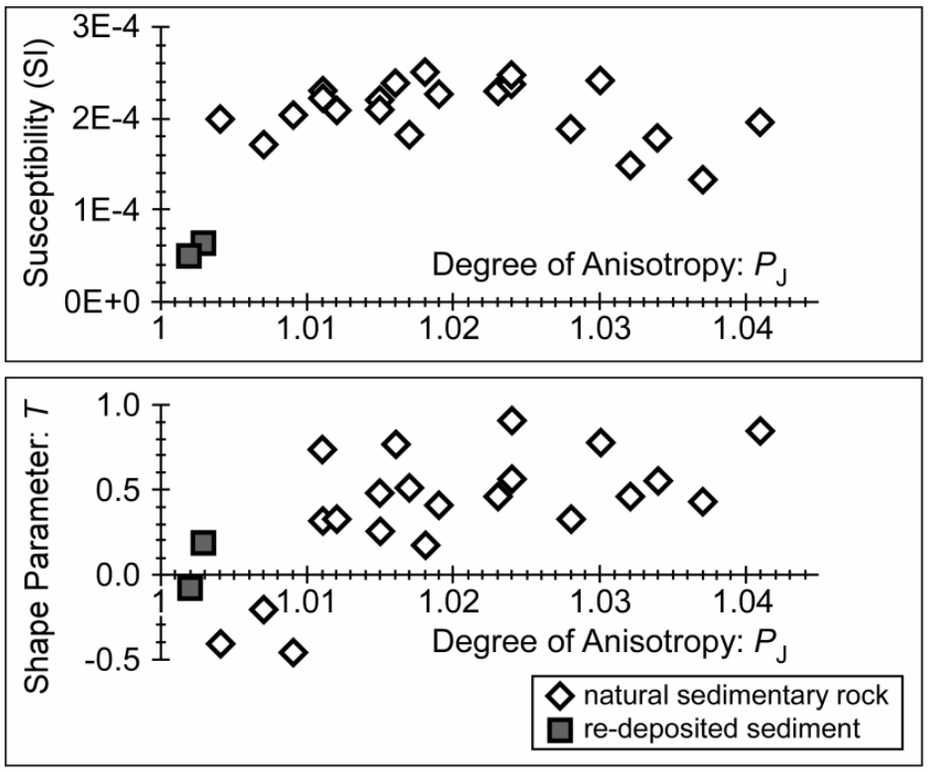

Figure 17. Magnitudes of magnetic fabrics in natural samples and re-deposited non-magnetic fine particles of the Kawabata Formation

5. Summary

Rock-magnetic investigation of sedimentary rocks provides insights into the basin's formation and sedimentation processes on an active margin. Cretaceous (Yezo Supergroup) ~ Eocene (Ishikari Group) strata and middle Miocene (Kawabata Formation) turbidites in central Hokkaido represent forearc and foreland settings, respectively. Progressive demagnetization successfully isolated characteristic remanent magnetization (ChRM) of the Kawabata Formation. Mean declination of the formation's ChRM exhibited significant westerly deflection, suggesting counterclockwise rotation of the study area since the middle Miocene. This differs from previous reports that indicated clockwise rotation. We attribute the difference to complicated deformation around the terminations of faults that form the N-S elongate Kawabata sedimentary basin. Anisotropy of magnetic susceptibility (AMS) principal axes were clearly determined for both the Cretaceous/Paleogene samples and Neogene samples, and regarded as a proxy of sediment influx directions. Paleocurrent directions inferred from the Eocene AMS data tend to align in N-S azimuth (Figure 14), and accord with the results of sedimentological paleoenvironment reconstruction, which suggest a northward downstream trend in fluvial to tidal estuarine systems [4]. As for the Cretaceous, further acquisition of AMS data is necessary to assess the effect of intensive syn-depositional deformation of the forearc [20]. After correcting for the tectonic rotation, most of the paleocurrent markers in the Kawa-

http://dx.doi.org/10.5772/56650

bata Formation indicated a westward current direction with minor southward flow contributions, consistent with a sedimentary model that envisions burial of the Miocene N-S foreland basin by clastics derived from the eastern collision front. The intensity of alignment forcing of sedimentary particles inferred from the shape parameter (T) of the AMS data was closely related to sedimentary facies observed in the field. In investigating the origin of the AMS fabrics of turbidite deposits of the Kawabata Formation, we conducted a re-deposition experiment of fine detrital particles with no magnetic fraction including paramagnetic minerals with relatively high magnetic susceptibility, which demonstrated the significance of the alignment of paramagnetic minerals having shape anisotropy.

Acknowledgements

The authors are grateful to N. Ishikawa for the use of the rock-magnetic laboratory at Kyoto University and for thoughtful suggestions in the course of the magnetic analyses. We thank S. Oshimbe and S. Nishizaki for their help with field work. Thanks are also due to N. Yamashita and Y. Danhara for their support in mineral separation. Constructive review comments by G. Kawakami greatly helped to improve early version of the manuscript.

Author details

Yasuto Itoh[1*], Machiko Tamaki[2] and Osamu Takano[3]

*Address all correspondence to: itoh@p.s.osakafu-u.ac.jp

1 Graduate School of Science, Osaka Prefecture University, Osaka, Japan

2 Japan Oil Engineering Co. Ltd., Tokyo, Japan

3 JAPEX Research Center, Japan Petroleum Exploration Co. Ltd., Chiba, Japan

References

[1] Editorial Committee of Hokkaido, Regional Geology of Japan. Regional Geology of Japan, Part 1: Hokkaido. Tokyo: Kyoritsu Shuppan; 1990.

[2] Tamaki M, Itoh Y. Tectonic implications of paleomagnetic data from upper Cretaceous sediments in the Oyubari area, central Hokkaido, Japan. Island Arc 2008; 17: 270-284.

[3] Tamaki M, Oshimbe S, Itoh Y. A large latitudinal displacement of a part of Cretaceous forearc basin in Hokkaido, Japan: paleomagnetism of the Yezo Supergroup in the Urakawa area. Journal of Geological Society of Japan 2008; 114: 207-217.

[4] Takano O, Waseda A. Sequence stratigraphic architecture of a differentially subsiding bay to fluvial basin: the Eocene Ishikari Group, Ishikari Coal Field, Hokkaido, Japan. Sedimentary Geology 2003; 160: 131-158.

[5] Takano O, Waseda A, Nishita H, Ichinoseki T, Yokoi K. Fluvial to bay-estuarine system and depositional sequences of the Eocene Ishikari Group, central Hokkaido. Journal of Sedimentological Society of Japan 1998; 47: 33-53.

[6] Miyasaka S, Hoyanagi K, Watanabe Y, Matsui M. Late Cenozoic mountain-building history in central Hokkaido deduced from the composition of conglomerate. Monograph of the Association for the Geological Collaboration in Japan 1986; 31: 285-294.

[7] Kawakami G, Yoshida K, Usuki T. Preliminary study for the Middle Miocene Kawabata Formation, Hobetsu district, central Hokkaido, Japan: special reference to the sedimentary system and the provenance. Journal of the Geological Society of Japan 1999; 105: 673-686.

[8] Otofuji Y, Kambara A, Matsuda T, Nohda S. Counterclockwise rotation of northeast Japan: paleomagnetic evidence for regional extent and timing of rotation. Earth and Planetary Science Letters 1994; 121: 503-518.

[9] Itoh Y, Tsuru T. Evolution history of the Hidaka-oki (offshore Hidaka) basin in the southern central Hokkaido, as revealed by seismic interpretation, and related tectonic events in an adjacent collision zone. Physics of the Earth and Planetary Interiors 2005; 153: 220-226.

[10] Takano O, Tateishi M, Endo M. Tectonic controls of a backarc trough-fill turbidite system; the Pliocene Tamugigawa Formation in the Niigata-Shin'etsu inverted rift basin, Northern Fossa Magna, central Japan. Sedimentary Geology 2005; 176: 247-279.

[11] Bouma AH. Sedimentology of Some Flysch Deposits; A Graphic Approach to Facies Interpretation. Amsterdam: Elsevier; 1962.

[12] Kawamura K, Ikehara K, Kanamatsu T, Fujioka K. Paleocurrent analysis of turbidites in Parece Vela Basin using anisotropy of magnetic susceptibility. Journal of the Geological Society of Japan 2002; 108: 207-218.

[13] Day R, Fuller M, Schmidt VA. Hysteresis properties of titanomagnetites: grain-size and compositional dependence. Physics of Earth and Planetary Interiors 1977; 13: 260-267.

[14] Kirschvink JL. The least-squares line and plane and the analysis of palaeomagnetic data. Geophysical Journal of the Royal Astronomical Society 1980; 62: 699-718.

[15] Kodama K, Takeuchi T, Ozawa T. Clockwise tectonic rotation of Tertiary sedimentary basins in central Hokkaido, northern Japan. Geology 1993; 21: 431-434.

[16] Takeuchi T, Kodama K, Ozawa T. Paleomagnetic evidence for block rotations in central Hokkaido-south Sakhalin, Northeast Asia. Earth and Planetary Science Letters 1999; 169: 7-21.

[17] Tamaki M, Kusumoto S, Itoh Y. Formation and deformation processes of late Paleogene sedimentary basins in southern central Hokkaido, Japan; paleomagnetic and numerical modeling approach. Island Arc 2010; 19: 243-258.

[18] Ledbetter MT, Ellwood BB. Spatial and temporal changes in bottom-water velocity and direction from analysis of particle size and alignment in deep-sea sediment. Marine Geology 1980; 38: 245-261.

[19] Tarling DH, Hrouda F. The Magnetic Anisotropy of Rocks. London: Chapman & Hall; 1993.

[20] Tamaki M, Tsuchida K, Itoh Y. Geochemical modeling of sedimentary rocks in the central Hokkaido, Japan: Episodic deformation and subsequent confined basin-formation along the eastern Eurasian margin since the Cretaceous. Journal of Asian Earth Sciences 2009; 34: 198-208.

IntechOpen

IntechOpen

IntechOpen